EDUSJ, Vol, 35, No: 3, 2026 (1 - 14)

Journal of Education and Science (ISSN 1812-125X)

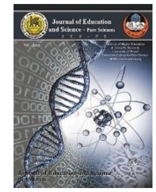

Study the Effectiveness of Automotive Glasses for Gamma Radiation Protection

M. T. Mohammod [1], M. A. Al-Jubbori [2*], A. E. Elzwam [3]

[1,2] Department of Physics, College of Education for Pure Science, University of Mosul, 41001, Mosul, Iraq
[3] Physics Department, College of Sciences, Tripoli University, Libya

Article information

Article history:
Received: December 22, 2025
Revised: February 28, 2026
Accepted: March 06, 2026
Available online: July 01, 2026

Keywords:
Radiation Protection Parameters
Car Windshield Glass
Gamma Ray Attenuation
Phy-X/PSD Program

Correspondence:
mushtaq_phy@uomosul.edu.iq

Abstract

In this study, four glass samples of the front car windows, the density of samples (2.2407-2.3868) g/cm³. The chemical composition of the samples was revealed using "energy-dispersive X-ray spectroscopy (EDS)". The samples consist of varying proportions of the elements (Na, Mg, C, O, Si). Radiation attenuation measurements were performed using gamma sources (Cs-137, Am-241, Ra-226) to study the shielding parameters of these samples. Found the linear attenuation coefficient (0.172-0.507) cm^{-1}, mass attenuation coefficient (0.0758-0.226) cm^2/g, half-value layer (1.367-4.126) cm, tenth-value layer (4.542-12.936) cm, mean free path (1.972-5.618) cm, transmittance factor (77.6-91.48) %, radiation shielding efficiency (8.5-22.4) %, effective atomic number (7.630-8.530), and effective electron number (3.00-3.118). The experimental results compared with results Phy-X software, and was good. The studied samples demonstrated a good efficiency in absorbing gamma rays at low energies, with performance comparable to standard protective materials such as certain types of glass and concrete. This type of glass represents a promising option in radiation protection applications that require transparent, lightweight, low-cost, and non-toxic materials, with the potential for further development to enhance its efficiency at higher energies.

DOI:10.33899/jes.v35i3.56204,

1. Introduction

Given the importance of radiation applications across in many fields, such as agriculture, industry, medicine, and scientific research, and despite these beneficial applications, radiation causes severe harm to humans and the environment if appropriate means of protection are not used [1], [2]. lead and lead-containing alloys are among the most important and best materials used in radiation protection. However, the use of these materials has disadvantages such as their lack of transparency, their large weight, and the damage caused by their toxicity. This prompted researchers to find alternatives for radiation protection that are non-toxic, safer, transparent, lightweight, inexpensive, sustainable, and easy to shape and modify in their components [3], [4], [5]. Many researchers have conducted studies on the gamma-ray blocking of many types of glass, such as barium borate glass and also fly ash glass [6], Lead borate glass [7], bismuth borate glass [8], phosphate glass containing Bi2O3, PbO, and BaO [9], lead and strontium borate glass [10], barium-bismuth-borosilicate glass [11], and silicate glass containing Bi2O3 [12], PbO-BaO-B2O3 glass [13], PbO-Li2O-B2O3 glass [14], heavy metal oxide glass, silicates and borates [15], and heavy metal oxide glass [16].

Authors have focused on using glass for shielding due to its unique properties such as transparency, electrical insulation, thermal stability, ease of shaping and preparation in large quantities, good spatial homogeneity, modification of its physical properties and chemical composition, and its ability to contain metal oxides such as (ZnO, Al_2O_3, SnO, PbO, Fe_2O_3, Bi_2O_3, WO_3), making it more effective in radiation protection [17], [18], [19], [20], [21][22], [23].

This study addressed the protective capacity against gamma rays of several samples of automotive windshields, where manufacturers create windshields consisting of two layers of tempered glass with a thin layer of plastic in between.
The shielding parameters of the samples were studied, including: linear attenuation coefficient (LAC), mass attenuation coefficient (MAC), half-value layer (HVL), tenth-value layer (TVL), effective atomic number (Zeff), effective electron number (Neff), transmission Factor (TF), radiation shielding efficiency (RPE), mean free path (MFP), over a within the specified energy range (0.060 - 0.662) MeV. To obtain the theoretical results, the Phy-X/PSD program was used and the difference with the practical results was noted to confirm experimental results and increase confidence. This study aims to use this type of glass as transparent, low-cost, and lead-free shields against gamma rays for radiation protection applications in industry, healthcare, and nuclear facilities.

This study aims to provide a comprehensive review of these traditional glasses and explore their potential as lead-free, reasonably priced al ternatives for radiation protection applications in industry, healthcare, and nuclear facilities.

2. Experiments and methodology

2.1. Materials and Sample Preparation

Four different samples of windshield glass from different car models were collected and each sample was given a specific code, The glass was cut using a glass cutting tool containing a small solid diamond-coated wheel, into rectangular pieces with an area of $(2 \times 1.5)\ \mathrm{cm}^2$ and different thicknesses as shown in Table 1. Then the surfaces were gently wiped, and each glass slide, the glass samples were washed and cleaned with distilled water, then with ethanol, and then dried in an oven at 80 degrees Celsius to remove any remaining moisture. The chemical composition was revealed using energy-dispersive X-ray spectroscopy (EDS) techniques of the samples and weight percentages (carbon, oxygen, sodium, magnesium, and silicon) were obtained.

Table 1: Model and Vehicle type

Sample	Vehicle type	Model	Thicknesses (cm)
S1	Chevrolet Aveo	2012	0.488
S2	SCANIA 112	1982	0.645
S3	Great Wall Deer	2012	0.503
S4	Opel	1994	0.497

a. **Density measurements**

A principle known as "Archimedes' principle" was applied to determine the density of the samples, at laboratory temperature using a density balance consisting of a highly sensitive balance (0.01 mg) and a density measurement kit. Using a density scale, the samples were weighed in the air and then while submerged in water. The density was calculated using equation [7]:

$$\rho = \frac{W_A}{W_A - W_B} \times \rho_{water} \qquad (1)$$

where W_A is the weight of the sample in air, W_B is the weight of the sample in distilled water, and ρ_{water} is the density of the distilled water.

Taking into account an experimental error of (±0.002) g/cm³, the measured density of the glass samples ranged between (2.2407 - 2.3868) g/cm³, reflecting slight variations in the proportions of the elements as shown in Table 2. These density values were also used in calculating the mass attenuation coefficients (MAC).

Table 2. Shows the chemical composition and density of the four glass samples.

Sample code	C	O	Na	Mg	Si	Density $\rho\ (g/cm^3)$ ∓ 0.002
S1	14.85	64.02	8.16	2.68	10.29	2.2407
S2	17.90	65.22	6.36	2.16	8.36	2.3173
S3	18.16	65.91	5.40	2.31	8.22	2.2921
S4	25.59	63.21	5.41	1.77	4.02	2.3868

b. **Gamma-ray attenuation measurements**

The protection parameters of the glass samples against gamma rays were measured spectroscopy system see Figure 1.a. The experimental setup used a NaI(Tl) flash detector with dimensions of 76 × 76 mm. (Bicron, USA) connected to a multichannel analyzer (MCA) via a preamplifier and a spectrometer. The tool is connected to a computer to analyze the data via specialized software. The detector was placed horizontally in a specific geometric arrangement at a distance of 15 cm from the source, and the collection time was 600 sec. The following sources were used: cesium-137 (188 kBc, half-life = 30.17 years), americium-241 (70 kBc, half-life = 432 years), and radium-226 (2.97 kBc, half-life = 1600 years) supplied by Amersham, were used as photon emitters. These sources provided Gamma photons within an energy range suitable for identifying the attenuation properties for the four samples, as illustrated in Figure 1. b.

The non-collision radiation intensity (I_0) was firstly recorded without any absorbing material in the beam path. Subsequently, the transmitted radiation intensity (I) was measured for each glass segment of known thickness (x). All measurements were performed at room temperature and under controlled background conditions.

Figure 1. (a) Gamma-ray spectroscopy system used to study the radiation protection standards for glass samples.
(b) – Standard sources of Cs-137, Am-241, and Ra-226.

The linear attenuation coefficient (LAC,μ) Calculates from "Beer-Lambert's law" [24]:

$$I = I_{\circ} e^{(-\mu x)} \quad (2)$$

Where ($I_{\circ}$) represent the incident and (I) represent transmitted photon intensities, and (x) represent of the sample thickness.

$$\text{or} \quad \mu = \ln(A/x) \quad (3)$$

Here, A is the attenuation ratio ($I_{\circ}/I$) [25].

Then, the mass attenuation coefficient (MAC) It is calculated from the following law[26]:

$$\mu_m\left(\frac{cm^2}{g}\right) = \frac{\mu\ (cm^{-1})}{\rho\ (\frac{g}{cm^3})} \quad (4)$$

To calculate the shielding parameters, the following relationships were used, which include the permeability factor (TF%), radiation protection efficiency (RPE%), half-valued layer (HVL), mean free path (MFP), tenth-value layer (TVL) [27], [17], [28]:

$$\mathrm{HVL(cm)} = \frac{\ln 2}{\mu} \quad , \qquad \mathrm{MFP(cm)} = \frac{1}{\mu} \qquad (5)$$

$$\mathrm{TVL(cm)} = \frac{\ln 10}{\mu} \qquad (6)$$

$$\mathrm{TF(\%)} = \frac{I}{I_0} \times 100 \qquad (7)$$

$$\mathrm{RPE} = \left(1 - \frac{I}{I_0}\right) \times 100 \qquad (8)$$

The effective atomic number (Zeff), where each element of the glass has a specific function [28].

$$Z_{eff} = \frac{\sum_i f_i \; A_i \; (\mu/\rho)_i}{\sum_i f_i \; \frac{A_i}{Z_i} \; (\mu/\rho)_i} \qquad (9)$$

Where $(\mu/\rho)_i$, fi, Zi and Ai are the mass attenuation coefficient, mean mole fraction, atomic number and atomic weight, respectively, of the constituent elements.

The effective number of electrons (Neff) of the samples was calculated from the following equation (8) [29]:

$$N_{eff} = \frac{N_A \, Z_{eff}}{\langle A \rangle} \qquad (10)$$

where N_A represent Avogadro's number, and $\langle A \rangle = \sum_i f_i A_i$ is the average atomic mass of the material [30].

2.4. Phy-X Calculations

Phy-X/PSD software was used to verify the experimental data, as this software can calculate Gamma-ray interaction coefficients such as mass attenuation coefficient (MAC), linear attenuation coefficient (LAC), half-layer value (HVL), mean free path (MFP), one-tenth layer value (TVL), and effective atomic number (Zeff), by entering the density of the sample or material into the program and its chemical composition [31]. The experimental and the theoretical results are present both together in Figure .3, which showed a high degree of agreement across the photon energy range under study (0.060–0.662) MeV.

3. Results and Discussion

The results of the density measurements between the glass samples showed (S1 – S4) had a slight difference in their density, with sample S1 showing the lowest density (2.2407 g/cm^3), while sample S4 showed the highest density (2.3868 g/cm^3). The density of sample S2 is (2.3173 g/cm3) and sample S3 is (2.2921 g/cm3). The slight difference in density is due to the proportions of elements present in the samples, Density is of great importance in radiation protection, as the efficiency of materials in attenuation increases with higher density, especially at high energies, as shown in Figure 2.

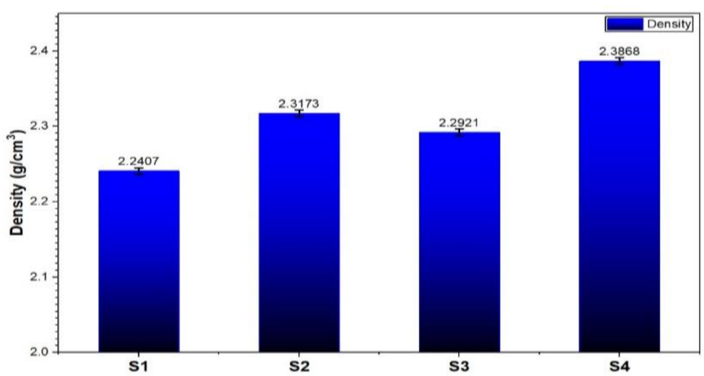

Figure 2. shows the density of the glass samples.

The relationship between the linear attenuation coefficient (LAC) of the glass samples (S1–S4) and the photon energy is evident from Figure 3, where the linear attenuation coefficient for all samples decreases with increasing photon energy. The explanation is that the photoelectric effect is the dominant mechanism in the low energy range, and the Compton effect prevails at medium and high energies. This leads to a gradual decrease in the LAC values. There appears to be good compatibility between the theoretical values of the Phy-x program and the experimental values for all samples, indicating the accuracy of the experimental measurements. The slight deviations at the energies (0.060–0.186) MeV are attributed to the sensitivity of the detector and the high experimental uncertainty. Sample S4 exhibits relatively high (LAC) values across most of the studied energy range. This is due to its relatively higher density. In general, the values of (LAC) are similar for all samples at all energies.

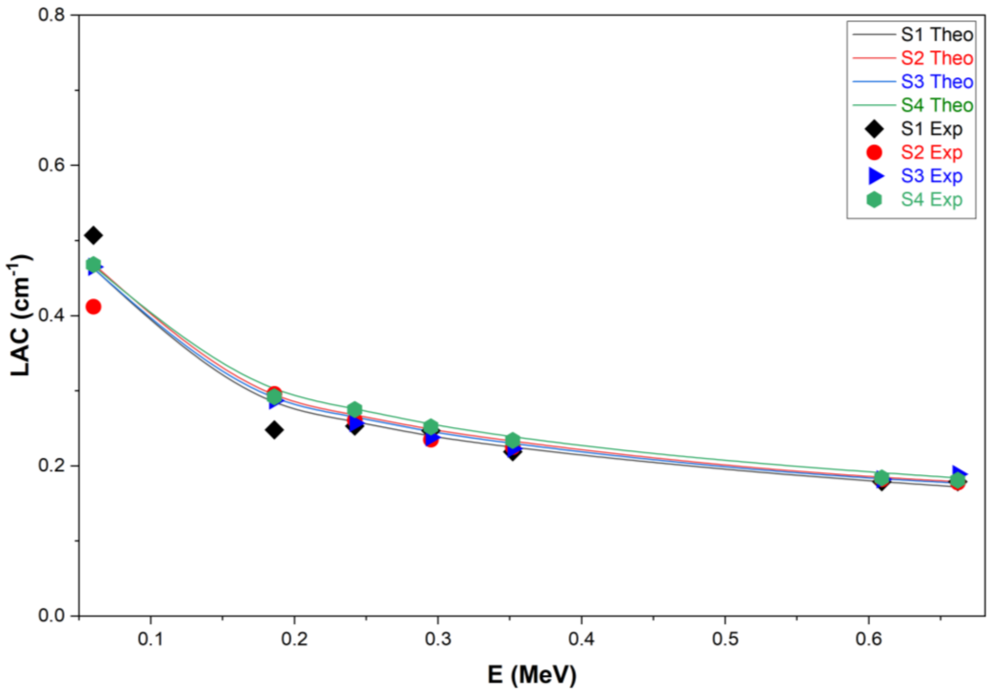

Figure 3. Theoretical and experimental values of the linear attenuation coefficient (LAC) in units of (cm^{-1}) at the studied gamma energy range in the four glass samples.

Table 3 shows a comparison between the experimental and theoretical values of the linear attenuation coefficient (LAC). The stander deviation between experimental and theoretical results ranged from 0.0% to 12.9%, yielding an average discrepancy of 3.05%. The RMSE value was 0.016 cm^{-1} further supports the excellent agreement between measured and calculated attenuation parameters, thereby validating the reliability of the experimental methodology.

Table 3. Table 2 shows the minor difference between experimental and theoretical values of the linear attenuation coefficient (LAC), in cm^{-1}, for glass samples.

E (MeV)	LAC (cm^{-1})											
	S1			S2			S3			S4		
	Theo	Exp	% Error	Theo	Exp	% Error	Theo	Exp	% Error	Theo	Exp	% Error
0.06	0.463	0.507	9.5	0.469	0.412	12.2	0.463	0.465	0.4	0.466	0.468	0.4
0.186	0.285	0.248	12.9	0.295	0.296	0.3	0.291	0.287	1.4	0.303	0.292	3.8
0.242	0.259	0.253	2.3	0.268	0.261	2.6	0.265	0.257	3.0	0.276	0.275	0.4
0.295	0.24	0.247	2.9	0.249	0.235	5.6	0.246	0.238	3.3	0.256	0.252	1.6
0.352	0.225	0.219	2.7	0.233	0.225	3.4	0.23	0.223	3.0	0.239	0.234	2.1
0.609	0.179	0.179	0	0.185	0.182	1.6	0.183	0.182	0.5	0.191	0.184	3.8
0.662	0.172	0.179	4.1	0.179	0.178	0.6	0.177	0.189	6.8	0.184	0.181	1.7

It is evident that (HVL), (TVL), and (MFP) respectively follow a similar behavior where they increase with increasing photon energies for all samples (S1-S4), which means a decrease in the efficiency of the glass samples for attenuation with a gradual increase in energy. Figures 4, 5, and 6 illustrate this. Sample S4 exhibits the lowest values for HVL, TVL, and MFP at most energies, indicating its high radiation attenuation efficiency. Conversely, sample S1 showed higher values for HVL, TVL, and MFP compared to the other samples. making it the least efficient at radiation attenuation. Generally, there are slight variations in HVL, TVL, and MFP values between the samples, attributable to their chemical composition and density within the energy range under study.

Figure 7 compares the (MFP) values of the current glass samples under study and materials that have recently undergone radiation protection studies, such as (12Bi2O3 12BaO 40SiO2 20ZnO 16Na2SO4), (12Bi2O3 12PbO2 40 SiO2 20ZnO 16Na2SO4), (30Bi2O3 30BaO 30 SiO2 5ZnO 5Na2SO4) [32], (Ordinary concrete), (Basalt - magnetite), and (Ilmenite) [33].

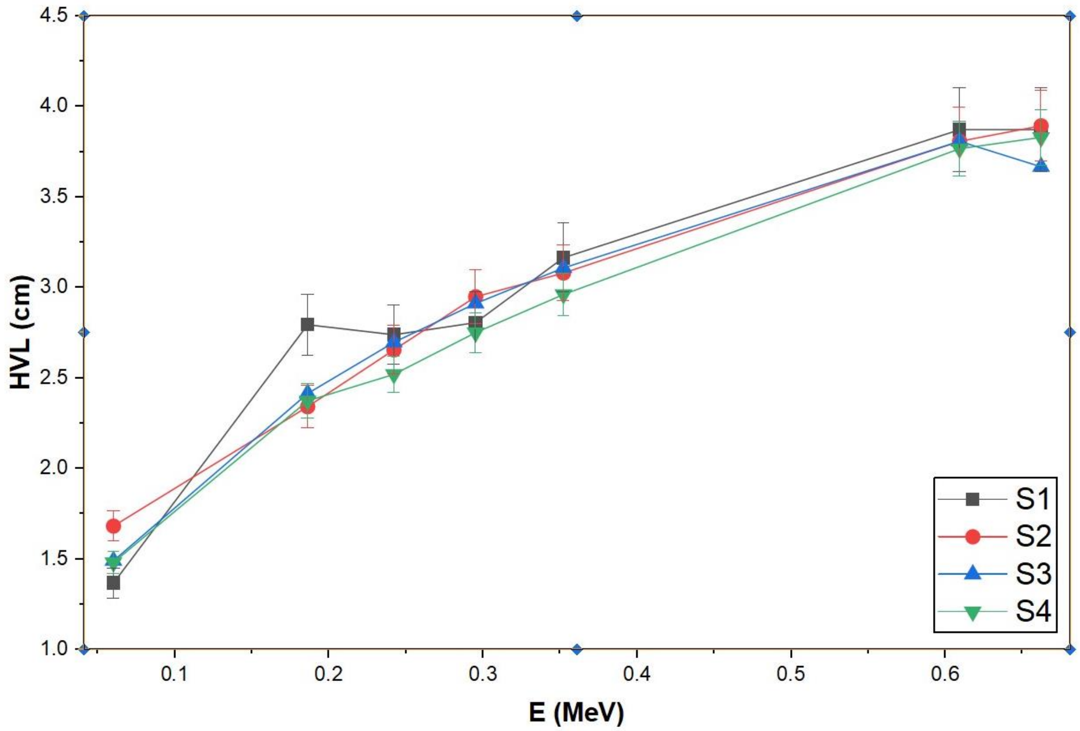

Figure 4. Half-value layer (HVL) for samples (S1-S4) at experimental gamma ray energies.

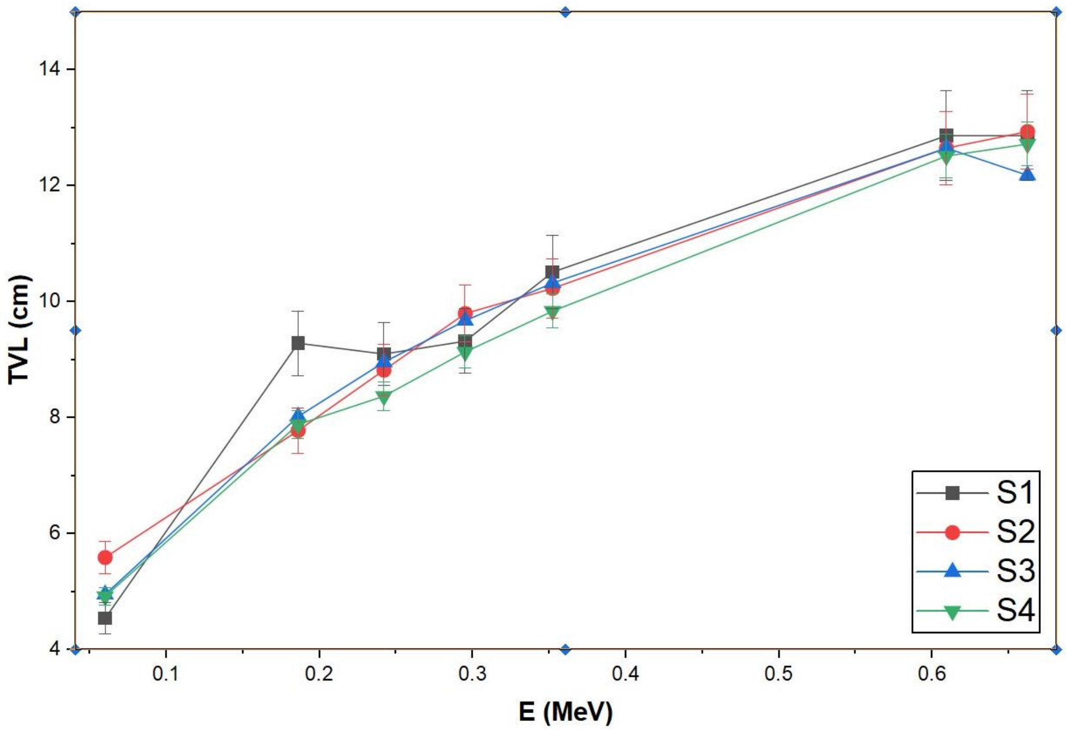

Figure 5. Tenth-Value Layer (TVL) for samples (S1-S4) at experimental gamma ray energies.

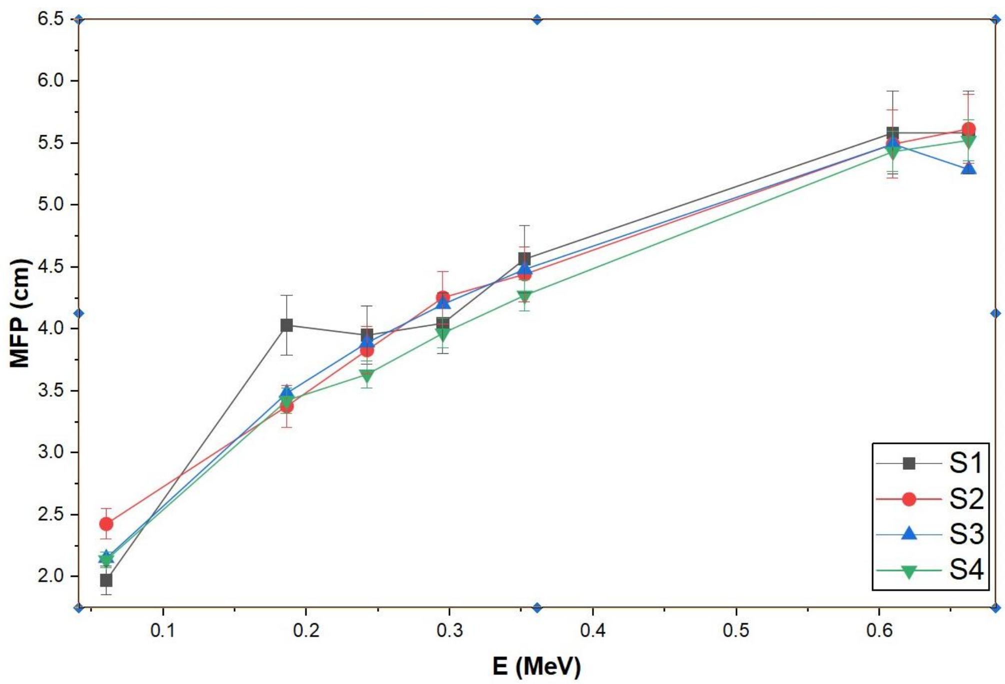

Figure 6. shows the mean free path (MFP) for samples (S1-S4) at experimental gamma ray energies.

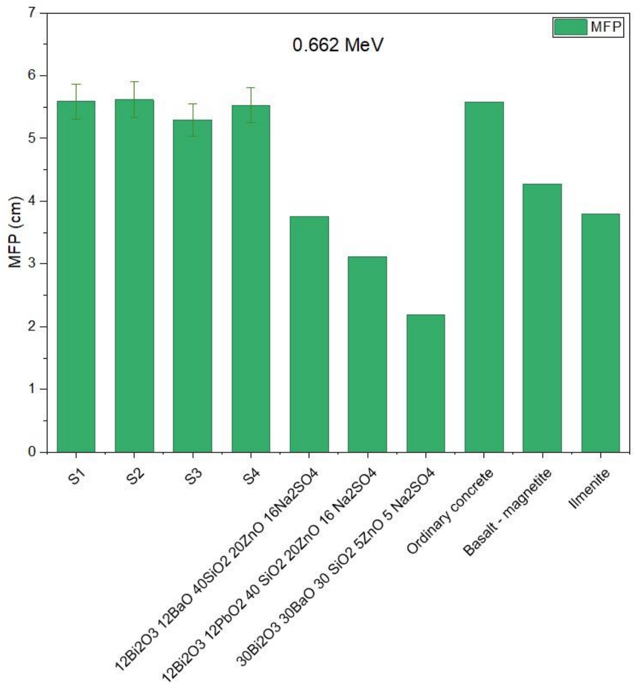

Figure 7. Comparison between the samples of the current study and 12Bi2O3 12BaO 40SiO2 20ZnO 16Na2SO4, 12Bi2O3 12PbO2 40 SiO2 20ZnO 16Na2SO4, 30Bi2O3 30BaO 30 SiO2 5ZnO 5Na2SO4, barite concrete, ordinary concrete, and ilmenite.

The relationship between the effective atomic number (Zeff) of the samples (S1-S4) in the energy range (0.060-0.662) MeV is illustrated in Figure 8, where the Zeff values of the samples show a decrease in the range (0.060-0.186) MeV. then become semi-stable with increasing energy. This decrease and subsequent stabilization is due to the photoelectric effect that prevails at low energy levels, which depends mainly on the atomic number of the elements contained in the samples. As the energy gradually increases, the probability of the photoelectric effect decreasing, and the Compton effect mechanism becomes more dominant until it is completely dominant at energy values higher than the studied energy range. The Compton effect is known to have a small dependence on atomic number, which leads to almost perfect stability in the (Zeff) values.

Sample S1 has relatively high Zeff values because it has higher proportions of elements with higher atomic numbers compared to the other samples, which means it features superior radiation protection capabilities. compared to the other samples. Sample S4 exhibits the lowest The protection against radiation is relatively low, as It is characterized by lower values for (Zeff) due to its lower content. of elements with higher atomic numbers. S1 and S2, on the other hand, show similar behavior due to their similar chemical composition.

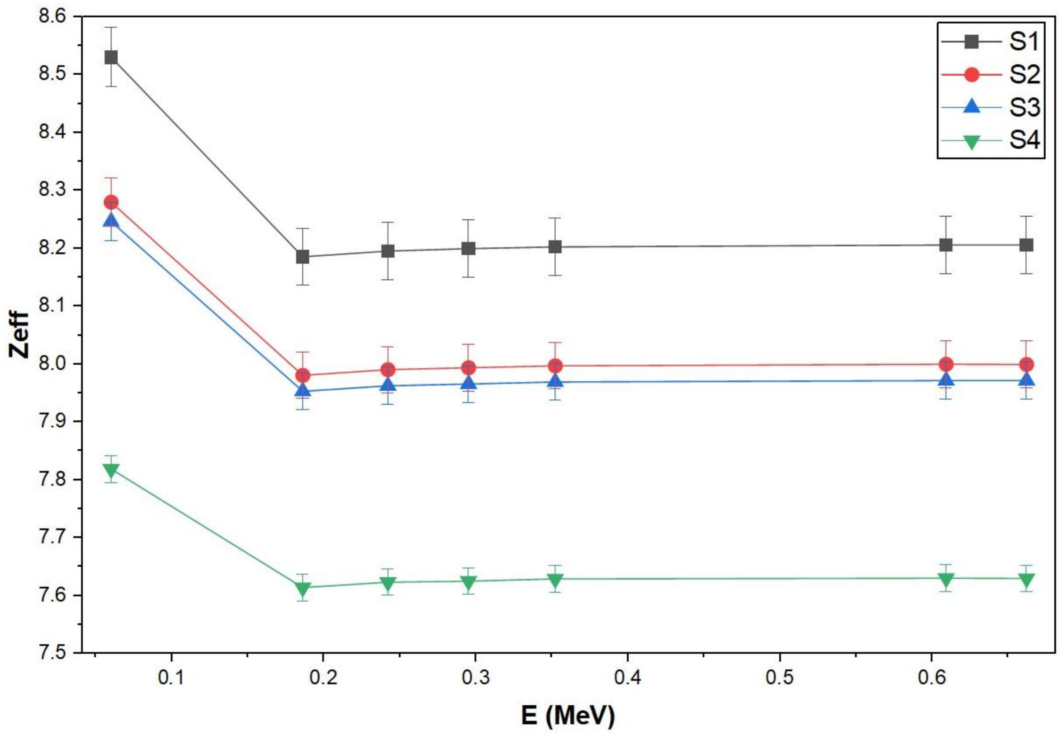

Figure 8. Shows the effective atomic number (Zeff) of samples (S1-S4) in the studied energy range of experimental gamma rays.

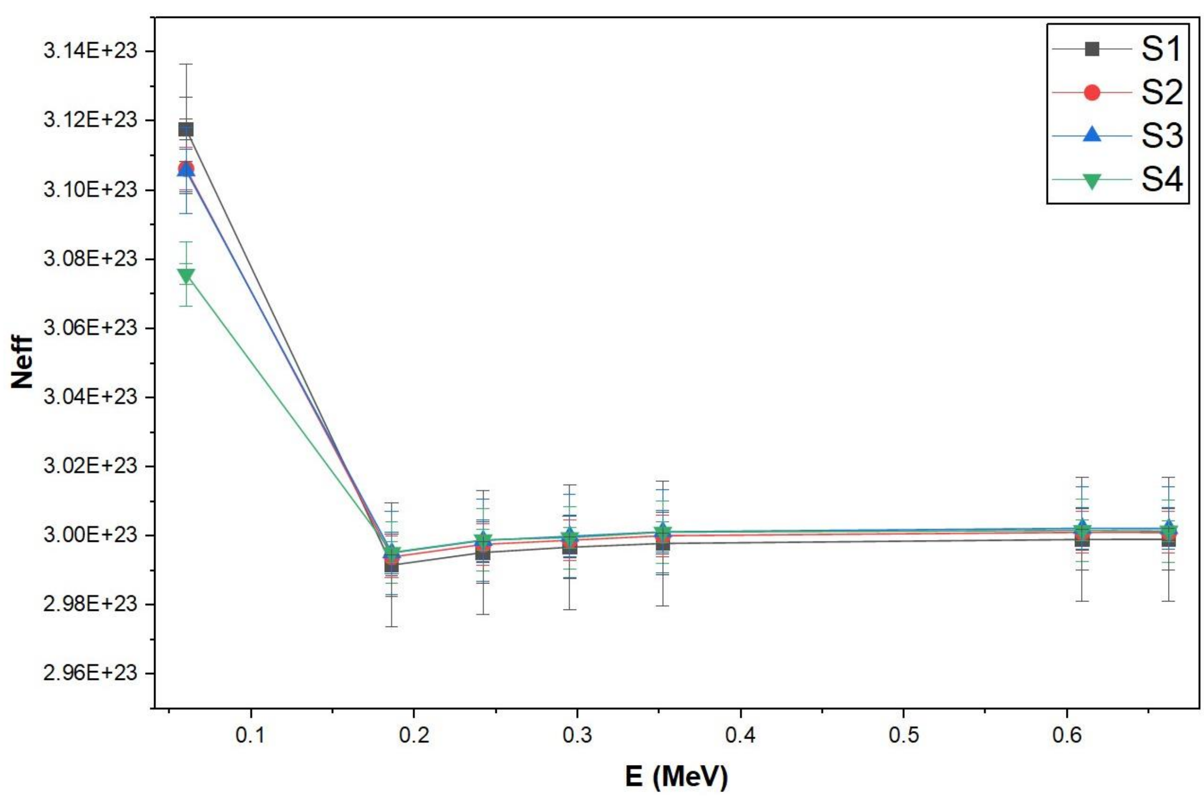

Figure 9. Shows the effective number of electrons (Neff) of glass samples at experimental gamma ray energies.

The effective number of electrons (Neff) changes with the gradual change in the energy of the incident photon in the range of (0.060-0.662) MeV for the studied glass. A sharp decrease in the value of (Neff) is observed in the lower energy range (0.060-0.186) MeV, as can be seen from Figure 9. This is because the probability of a photoelectric effect decreasing as the photon energy gradually increases. At low energies, the photoelectric absorption coefficient is high, leading to higher Neff values in this part of the spectrum. Sample S1 shows relatively high Neff values, while sample S4 shows relatively low values. This indicates that there are differences in chemical composition and electron density between these samples.
In the higher energy range (0.186–0.662) MeV, near-perfect stability is observed in the Neff values for all samples and that is the effect of the dominant Compton reaction in that range, the Compton effect is mainly affected by the number of free electrons within the material., which explains the near-consistency of the Neff with increasing energy in this part of the spectrum.

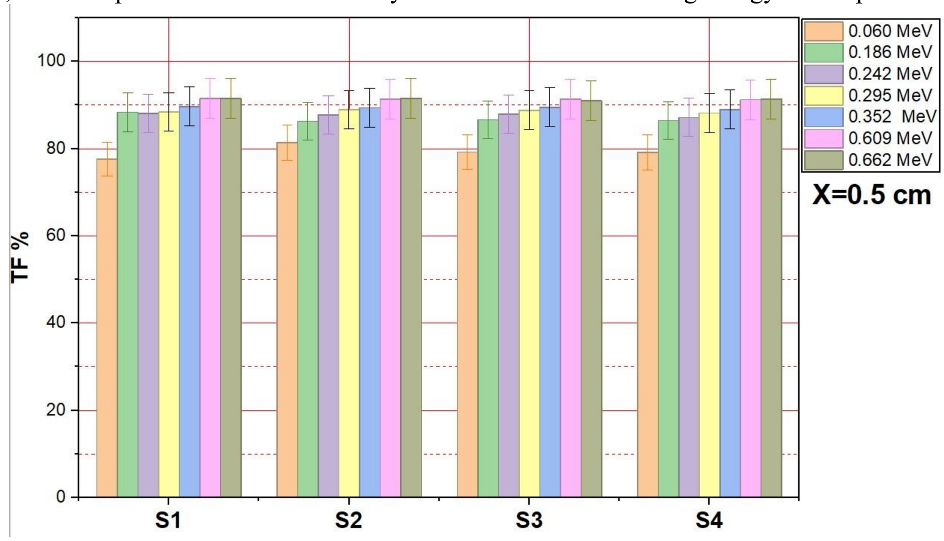

Figure 10. shows the change in the transmittance factor (TF%) of the samples with the change in experimental gamma ray energy.

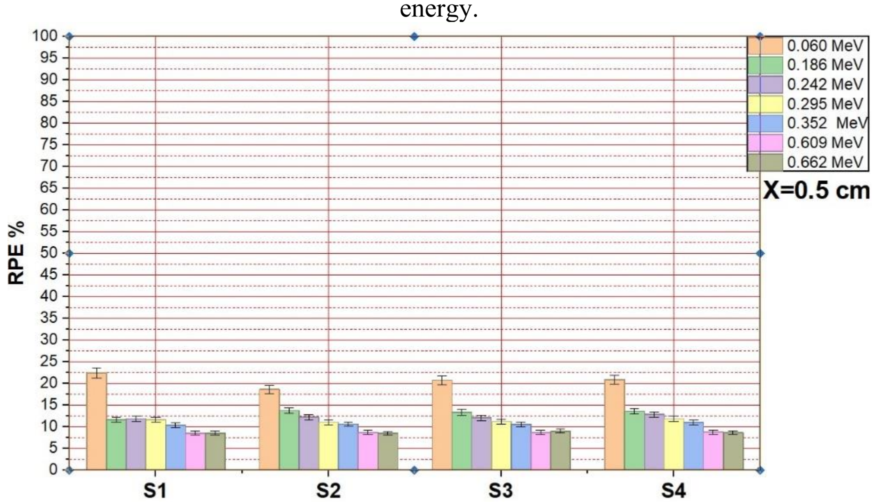

Figure 11. illustrates the change in radiation protection efficiency (RPE%) of the samples with the change in experimental gamma ray energy.

It is clear the percentage of transmitted radiation (TF%) through the samples (S1-S4) when the energy is changed within the range (0.060-0.662) MeV. That there is a distinct dependence on energy, as the percentage of photon transmission increases with increasing energy for all samples As shown in Figure 10, while figure 11 illustrates the radiation protection efficiency (RPE%) values for glass (S1-S4) as the incident photon energy increases in the range (0.060-0.662) MeV. A gradual decrease in RPE% is observed with a gradual increase in energy. At an energy of (0.060) MeV, RPE% ranges between (18.62-22.39) %, while at an energy of (0.662) MeV, it decreases to approximately (8.51-9)%. These results indicate better radiation shielding efficiency for the samples at lower energies. The increase in TF% and decrease in RPE% with increasing energy is explained by the dominant absorption mechanism and the chemical composition and density of the samples. Sample S1 exhibits the lowest

TF% and highest RPE% at low energies. As the energy increases, RPE% decreases and TF% increases compared to the other samples, due to its relatively lower density and higher content of (Mg, Si, Na). Sample S4, on the other hand, shows a slight increase in RPE% and a slight decrease in TF% with increasing energy compared to the other samples, due to its relatively higher density, which improves its performance at higher energy levels compared to the other samples.

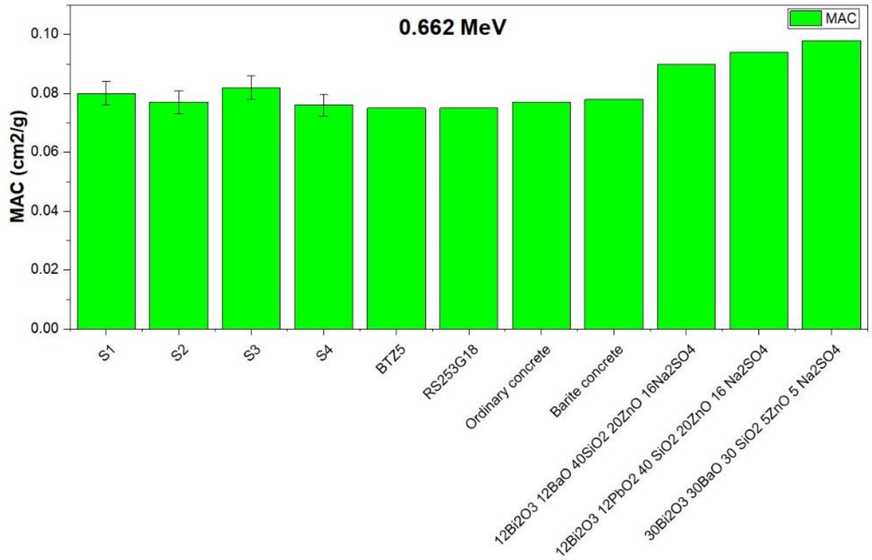

Figure 12. Comparison of samples (S1-S4) with a number of previous studies of several types of glass and concrete used in radiation shielding at energy levels (0.662 MeV).

Figure 12 shows a comparison between the results of the Mass Attenuation Coefficient (MAC) for the studied glass samples and previous studies. The MAC values for samples (S1–S4) at an energy of (0.662) MeV ranged between 0.076 and 0.082 cm²/g, with all samples showing statistically similar values to other commercial and reference bottles. For example, the MAC values for two types of glass, BTZ5 and RS253G18, were determined to be 0.075 cm²/g [34], [2],bismuth-containing sodium silicate glass (0.090) cm²/g, lead oxide-containing sodium silicate glass (0.094) cm²/g, and barium-containing sodium silicate glass (0.098) cm²/g [32], and similarly these values for the glass systems shown are very similar to those of ordinary concrete (0.077 cm²/g) and barite-containing concrete (0.078 cm²/g) [35], both materials used for radiation shielding. These results are very close to the values of the studied samples and the similar glass system in previous studies; therefore, it follows from what has been mentioned above that the glass samples currently under study have a radiation attenuation effect similar to that of materials used in shielding and can be used as protective shields at low energies.

4. Conclusion

It is concluded from this study that the glass samples (S1-S4) taken from of the front car windshield had their densities determined using Archimedes' principle and their values ranged approximately between (2.2407–2.3868) g/cm^3. Using energy-dispersive X-ray spectroscopy (EDS), the chemical composition of the glass samples was identified, revealing that they consist of varying proportions of elements (Na, Mg, C, O, Si). Radioactive attenuation measurements were performed using gamma sources (Cs-137, Am-241, Ra-226) to study the shielding parameters of these samples, within the energy range (0.06-0.662) MeV.

It had relatively good radiation attenuation performance, and the chemical composition and density had a clear effect on the experimental results, as the S4 sample, which had the highest density at most energies, showed a high value for (LAC) and low values for (HVL), (TVL) and (MFP) compared to the other samples, indicating better performance in radiation protection efficiency and transmission reduction. However, sample S1 showed lower (LAC) and higher (HVL), (TVL), and (MFP), indicating lower attenuation efficiency than the other samples.

The results also showed that (Zeff) and (Neff) gradually decrease at low energies, which is explained by the dominance of the photoelectric effect, and then almost complete stability is achieved at higher energies due to the increased occurrence of the Compton effect. The experimental results showed good convergence of the linear attenuation coefficient with the theoretical results of Phy-X, which increases the credibility of the experimental measurements. Comparison of the results with previous studies of materials and glass used confirmed that the (MAC) and (MFP) values of the studied samples fall within the acceptable range for materials used in radiation applications at low energies.

The results generally indicate that the automotive glass under study exhibits good attenuation efficiency at low energies. It confirms its potential use as suitable alternatives as transparent, lightweight, lead-free, and low-cost radiation shields, as it can be used in many applications that require both radiation protection and transparency, such as windows in laboratories, and transparent personal protective equipment for monitoring experiments, handling radiation sources in laboratories safely, and radiographic imaging applications.

5. Declarations

5.1 Ethics approval and consent to participate:
Not applicable.

5.2 Consent for publication: I agree

5.3 Availability of Data and Materials:
Data will be provided upon receiving a valid request.

5.4 Conflicts of interest:
The authors declare that there is no conflict of interest

5.5 Funding:
The authors declare that they have no known competing financial interests or personal relationships that could have appeared to influence the work reported in this paper.

5.6 Acknowledgments:
The authors would like to express their appreciation to warmest thanks to the University of Mosul, College of Education for Pure Science, Department of Physics for supporting this work. for supplying the materials for this study.

5. References

[1] M. Kurudirek, N. Chutithanapanon, R. Laopaiboon, C. Yenchai, and C. Bootjomchai, “Effect of Bi2O3 on gamma ray shielding and structural properties of borosilicate glasses recycled from high pressure sodium lamp glass,” *J. Alloys Compd.*, vol. 745, pp. 355–364, 2018, doi: 10.1016/j.jallcom.2018.02.158.

[2] P. Kaur, K. J. Singh, S. Thakur, P. Singh, and B. S. Bajwa, “Investigation of bismuth borate glass system modified with barium for structural and gamma-ray shielding properties,” *Spectrochim. Acta - Part A Mol. Biomol. Spectrosc.*, vol. 206, pp. 367–377, 2019, doi: 10.1016/j.saa.2018.08.038.

[3] C. Doering and S. Colmanet, “The Australian Radiation Protection and Nuclear Safety Agency,” *Aust. Phys.*, vol. 47, no. 1, pp. 9–13, 2010.

[4] A. A. S. Esmail, M. M. Kassab, M. M. Radwan, and M. A. Abd-Latif, “Radiation shielding properties of xPbF2−20Na2O−10CaO−(70−x) B2O3 glass system,” *Edelweiss Appl. Sci. Technol.*, vol. 9, no. 2, pp. 2208–2223, 2025, doi: 10.55214/25768484.v9i2.5058.

[5] N. Karpuz, “Radiation shielding properties of glass composition,” *J. Radiat. Res. Appl. Sci.*, vol. 16, no. 4, p. 100689, 2023, doi: 10.1016/j.jrras.2023.100689.

[6] S. Singh, A. Kumar, D. Singh, K. S. Thind, and G. S. Mudahar, “Barium-borate-flyash glasses: As radiation shielding materials,” *Nucl. Instruments Methods Phys. Res. Sect. B Beam Interact. with Mater. Atoms*, vol. 266, no. 1, pp. 140–146, 2008, doi: 10.1016/j.nimb.2007.10.018.

[7] K. Kirdsiri, J. Kaewkhao, A. Pokaipisit, W. Chewpraditkul, and P. Limsuwan, “Gamma-rays shielding properties of xPbO:(100 - x)B2O3 glasses system at 662 keV,” *Ann. Nucl. Energy*, vol. 36, no. 9, pp. 1360–1365, 2009, doi: 10.1016/j.anucene.2009.06.019.

[8] K. Singh *et al.*, “Gamma-ray attenuation coefficients in bismuth borate glasses,” *Nucl. Instruments Methods Phys. Res. Sect. B Beam Interact. with Mater. Atoms*, vol. 194, no. 1, pp. 1–6, 2002, doi: 10.1016/S0168-583X(02)00498-6.

[9] J. Kaewkhao and P. Limsuwan, “Mass attenuation coefficients and effective atomic numbers in phosphate glass containing Bi2O3, PbO and BaO at 662 keV,” *Nucl. Instruments Methods Phys. Res. Sect. A Accel. Spectrometers, Detect. Assoc. Equip.*, vol. 619, no. 1–3, pp. 295–297, 2010, doi: 10.1016/j.nima.2009.11.033.

[10] R. S. Kaundal, S. Kaur, N. Singh, and K. J. Singh, “Investigation of structural properties of lead strontium borate glasses for gamma-ray shielding applications,” *J. Phys. Chem. Solids*, vol. 71, no. 9, pp. 1191–1195, 2010, doi: 10.1016/j.jpcs.2010.04.016.

[11] C. Bootjomchai, J. Laopaiboon, C. Yenchai, and R. Laopaiboon, “Gamma-ray shielding and structural properties of barium-bismuth-borosilicate glasses,” *Radiat. Phys. Chem.*, vol. 81, no. 7, pp. 785–790, 2012, doi:

10.1016/j.radphyschem.2012.01.049.

[12] N. Chanthima and J. Kaewkhao, "Investigation on radiation shielding parameters of bismuth borosilicate glass from 1 keV to 100 GeV," *Ann. Nucl. Energy*, vol. 55, pp. 23–28, 2013, doi: 10.1016/j.anucene.2012.12.011.

[13] S. A. M. Issa, "Effective atomic number and mass attenuation coefficient of PbO-BaO-B2O3 glass system," *Radiat. Phys. Chem.*, vol. 120, pp. 33–37, 2016, doi: 10.1016/j.radphyschem.2015.11.025.

[14] A. Kumar, "Gamma ray shielding properties of PbO-Li2O-B2O3 glasses," *Radiat. Phys. Chem.*, vol. 136, pp. 50–53, 2017, doi: 10.1016/j.radphyschem.2017.03.023.

[15] V. P. Singh, N. M. Badiger, and J. Kaewkhao, "Radiation shielding competence of silicate and borate heavy metal oxide glasses: Comparative study," *J. Non. Cryst. Solids*, vol. 404, pp. 167–173, 2014, doi: 10.1016/j.jnoncrysol.2014.08.003.

[16] V. P. Singh, M. E. Medhat, and N. M. Badiger, "Photon attenuation coefficients of thermoluminescent dosimetric materials by Geant4 toolkit, XCOM program and experimental data: A comparison study," *Ann. Nucl. Energy*, vol. 68, pp. 96–100, 2014, doi: 10.1016/j.anucene.2014.01.011.

[17] A. Saleh, M. G. El-Feky, M. S. Hafiz, and N. A. Kawady, "Experimental and theoretical investigation on physical, structure and protection features of TeO2–B2O3 glass doped with PbO in terms of gamma, neutron, proton and alpha particles," *Radiat. Phys. Chem.*, vol. 202, p. 110586, 2023, doi: 10.1016/j.radphyschem.2022.110586.

[18] M. I. Sayyed, A. Saleh, A. Kumar, and F. E. Mansour, "Experimental examination on physical and radiation shielding features of boro-silicate glasses doped with varying amounts of BaO," *Nucl. Eng. Technol.*, vol. 56, no. 8, pp. 3378–3384, 2024.

[19] A. Saleh, "Comparative shielding features for X/Gamma-rays, fast and thermal neutrons of some gadolinium silicoborate glasses," *Prog. Nucl. Energy*, vol. 154, p. 104482, 2022, doi: 10.1016/j.pnucene.2022.104482.

[20] A. Saleh, R. Elshazly, and H. Abd Elghany, "The impact of CdO on the radiation shielding properties of zinc-sodium-phosphate glass containing barium," *Arab J. Nucl. Sci. Appl.*, vol. 55, no. 1, pp. 116–126, 2022.

[21] A. A. Saleh and B. M. Mahmoud, "A Simulation Study: Radiation Shielding Performance of Dy/Eu-Doped Boro-FBi Glasses," *Egypt. J. Biomed. Eng. Biophys.*, vol. 26, no. 1, 2025.

[22] A. Saleh *et al.*, "Optimizing the integration between radiation protection optical, and mechanical strength for advanced nuclear safety applications using tungsten-doped Bismuth Borate Glasses," *Radiat. Phys. Chem.*, p. 113216, 2025.

[23] A. Saleh, M. I. Sayyed, A. Kumar, and F. E. Mansour, "Synthesis and gamma-ray shielding efficiency of borosilicate glasses doped with zinc oxide: comparative study," *Silicon*, vol. 16, no. 10, pp. 4427–4435, 2024.

[24] A. Saleh, R. Elshazly, and H. Abd Elghany, "The Impact of CdO on the Radiation Shielding Properties of Zinc-Sodium-Phosphate Glass Containing Barium," *Arab J. Nucl. Sci. Appl.*, vol. 0, no. 0, pp. 1–11, 2021, doi: 10.21608/ajnsa.2021.80370.1478.

[25] L. A. Najam, A. K. Hashim, H. A. Ahmed, and I. M. Hassan, "Study the Attenuation Coefficient of Granite to Use It as Shields against Gamma Ray," *Detection*, vol. 04, no. 02, pp. 33–39, 2016, doi: 10.4236/detection.2016.42005.

[26] A. Shahboub, G. El Damrawi, and A. Saleh, "A new focus on the role of iron oxide in enhancing the structure and shielding properties of Ag2O–P2O5 glasses," *Eur. Phys. J. Plus*, vol. 136, no. 9, p. 947, 2021, doi: 10.1140/epjp/s13360-021-01948-1.

[27] A. Shahboub, A. Saleh, A. K. Hassan, and G. El Damrawi, "EPR studies and radiation shielding properties of silver aluminum phosphate glasses," *Appl. Phys. A Mater. Sci. Process.*, vol. 129, no. 6, p. 410, 2023, doi: 10.1007/s00339-023-06681-3.

[28] M. I. Sayyed *et al.*, "Experimental investigation on tuning radiation shielding competence in magnesium-germanium-boro-tellurite glasses modified with PbO," *Results Mater.*, vol. 28, p. 100817, Nov. 2025, doi: 10.1016/j.rinma.2025.100817.

[29] G. Susoy *et al.*, "The impact of Cr2O3 additive on nuclear radiation shielding properties of LiF–SrO–B2O3 glass system," *Mater. Chem. Phys.*, vol. 242, p. 122481, 2020, doi: 10.1016/j.matchemphys.2019.122481.

[30] S. R. Manohara, S. M. Hanagodimath, and L. Gerward, "Photon interaction and energy absorption in glass: A transparent gamma ray shield," *J. Nucl. Mater.*, vol. 393, no. 3, pp. 465–472, 2009, doi: 10.1016/j.jnucmat.2009.07.001.

[31] E. Şakar, Ö. F. Özpolat, B. Alım, M. I. Sayyed, and M. Kurudirek, "Phy-X / PSD: Development of a user friendly online software for calculation of parameters relevant to radiation shielding and dosimetry," *Radiat. Phys. Chem.*, vol. 166, p. 108496, 2020, doi: 10.1016/j.radphyschem.2019.108496.

[32] A. Ali, W. Zeyara, S. Nagem, E. Jumha, and T. Fayez, "A comparative study of gamma radiation shielding parameters for sodium silicate glass containing bismuth, barium and lead oxide in the energy range (0.6–1.5 MeV)," *Wadi Alshatti Univ. J. Pure Appl. Sci.*, vol. 2, no. 1, pp. 16–22, 2024.

[33] N. F. Rozi, L. Hasnimulyati, and A. Azuraida, "Simulated radiation shielding parameter for energy 1 keV-100 GeV of lead-free borotellurite based glass for nuclear medicine application," *Chalcogenide Lett.*, vol. 22, no. 1, pp. 57–76, 2025, doi: 10.15251/CL.2025.221.57.

[34] P. Limkitjaroenporn, J. Kaewkhao, P. Limsuwan, and W. Chewpraditkul, "Physical, optical, structural and gamma-ray shielding properties of lead sodium borate glasses," *J. Phys. Chem. Solids*, vol. 72, no. 4, pp. 245–251, 2011, doi: 10.1016/j.jpcs.2011.01.007.

[35] Y. B. Saddeek, E. R. Shaaban, E. S. Moustafa, and H. M. Moustafa, "Spectroscopic properties, electronic polarizability, and optical basicity of Bi2O3-Li2O-B2O3 glasses," *Phys. B Condens. Matter*, vol. 403, no. 13–16, pp. 2399–2407, 2008, doi: 10.1016/j.physb.2007.12.027.

دراسة فعالية زجاج السيارات للحماية من اشعة كاما

محمود طه محمد [1]، مشتاق عبد داود الجبوري[2]، عياد الهادي الزوام[3]

[1,2] قسم الفيزياء، كلية التربية للعلوم الصرفة، جامعة الموصل، الموصل، العراق

[3] قسم الفيزياء، كلية العلوم، جامعة طرابلس، ليبيا

الخلاصة:

في هذه الدراسة، تم تحليل أربع عينات زجاجية من النوافذ الأمامية للسيارات، بكثافة تتراوح بين (2.2407– 2.3868) جرام/سم^3. وتم الكشف عن التركيب الكيميائي باستخدام التحليل الطيفي للأشعة السينية المشتتة من الطاقة (EDS) تتكون هذه العينات الزجاجية من نسب متفاوتة من العناصر (C, O, Si Mg, Na). وتم إجراء قياسات التوهين الإشعاعي باستخدام مصادر غاما(Cs-137، Am-241، Ra-226) لدراسة معلمات التدريع لهذه العينات ووجد أن معامل التوهين الخطي (0.172-0. 0.507) سم$^{-1}$، معامل التوهين الكتلي (0.0758-0.226) سم^2/جم، طبقة نصف القيمة (1.367-4.126) سم، طبقة القيمة العاشرة (4.542-12.936) سم، متوسط المسار الحر (1.972-5.618) سم، عامل النفاذية (77.6-91.48)%، كفاءة الحماية من الإشعاع (8.5-22.4)%، العدد الذري الفعال (7.630-8.530)، والرقم الإلكتروني الفعال (3.00-3.118)، وقورنت النتائج التجريبية ببرنامج بنتائج Phy-X، وكانت النتائج جيدة عند الطاقات الواطئة بأداء مقارب للمواد القياسية المستخدمة في الحماية مثل أنواع معينة من الزجاج والخرسانة. ويمثل هذا النوع من الزجاج خياراً واعداً في تطبيقات الحماية الإشعاعية التي تتطلب موادًا شفافة، خفيفة، منخفضة التكلفة، وغير سامة، مع إمكانية تطوير إضافي لتعزيز كفاءتها عند الطاقات الأعلى.